




Evaluating Mesh Geometry and Shade Coefficient for Fog Harvesting Collectors

Abdullah A. Elshennawy^{1,2} · Magdy Y. Abdelaal³ · Ahmed M. Hamed¹ · Mohamed M. Awad¹ 

Received: 11 March 2023 / Accepted: 14 October 2023 / Published online: 14 November 2023
© The Author(s) 2023

Abstract

The most valuable resource for sustaining life on earth is water. In dry and semi-arid areas, the problem of water scarcity can be resolved with the aid of fog collection techniques employing fog collectors. Fog collection is greatly influenced by a variety of factors. Some are design parameters, while others depend on ambient circumstances. Geometry and the mesh's shade coefficient are important design factors that can be modified and have an impact on the rate at which fog collects in fog collectors. The shape of the mesh holes and the process used to create the mesh serve to identify geometry and measure the shade coefficient. In this paper, a straightforward mathematical technique is proposed to make it easier to calculate the shade coefficient of various mesh shapes used in fog harvesting and to provide an approximation of the mesh volume and cost. Five alternative geometries were used: the rectangular mesh, square mesh, Raschel mesh, triangular mesh, and hexagonal mesh. The current simple method will facilitate the design of the fog mesh collector and can assist in achieving the ideal shade coefficient and most effective mesh geometry for fog harvesting. Rectangular meshes were solely used as an example to evaluate the results. Stainless steel rectangular meshes with various shade coefficients were tested for fog collection, and the amount of water collected by each mesh varied. It was concluded that the optimum shade coefficient ranged 50–60% for fog collection.

Keywords Shade coefficient · Fog harvesting · Mesh geometry · Rectangular mesh · Raschel mesh · Hexagonal mesh

Nomenclature

A_f	Mesh openings area, m ²
A_{hex}	Area of hexagon, m ²
A_t	Total mesh area, m ²
a	Mesh width, m
b	Mesh height, m
C_o	Mesh pressure drop coefficient
C_d	Collector drag coefficient
d	Mesh depth, m
D	Rectangular fiber diameter, m

n_x	Number of holes per horizontal row
n_y	Number of holes per vertical column
s	Shade coefficient
t	Mesh fiber thickness, m
v	Mesh material volume, m^3
x	Rectangular and hexagonal mesh hole length, m
x_b	Trapezium bigger base, m
x_s	Trapezium smaller base, m
y	Rectangular, triangular and hexagonal mesh hole height, m
η_{ac}	Aerodynamic collection efficiency

1 Introduction

Water scarcity is a devastating crisis that is engulfing people in arid regions; access to fresh water is becoming increasingly traumatic (Chitsaz and Azarnivand 2017). Over 66% of the world's population experiences water shortages for one entire month spaced across the year (Mekonnen and Hoekstra 2016). Many nations that currently have enough water will have been affected by the situation by 2030 (Rijsberman 2006). Therefore, it is recommended to better use water resources and reduce greenhouse gases in many countries like Gulf Cooperation Council (GCC) countries (Alotaibi et al. 2023).

There are different methods to overcome water scarcity including fog collection, desalination and water extraction from air. For instance, water extraction from air using solar energy and $CaCl_2$ solution was performed in Mansoura university via double slope condensation surface (Awad et al. 2020), portable apparatus (Talaat et al. 2018), and foldable apparatus (Fathy et al. 2020). To minimize the size of the droplets so that the heated distillate droplets may only flow against gravity, Abu El-Maaty et al. (Abu El-Maaty et al. 2019, 2021) used a fogging system to desalinate seawater with solar system integration. In addition, for researchers who strive to make better and wiser use of water resources, fog harvesting is a great issue of interest for water resources developers. Fog collection was evaluated experimentally in Saudi Arabia in three different regions to collect water from fog where there were big differences between each place's collection rate (Al-hassan 2009). Therefore, the fog collection rate mainly depends on the region. However, many parameters also influence the performance of fog harvesting that can be human-controlled (Elshennawy et al. 2022). Mesh geometry comes first. Rajaram et al. 2016) investigated the water transport route on the fibers of rectangular and Raschel mesh. they discovered that the rectangular mesh had more difficulties with water transport, causing water droplets accumulation on the holes and reducing the shade coefficient due to hole blockage. Raschel mesh, on the other hand, is more convenient and demonstrated better water droplets coalescence and transport. Secondly, Mesh material is definitely a crucial controlling factor. Inspired by the lotus effect (Guo et al. 2011). High water contact angle surfaces are more advantageous for fog collection due to their superhydrophobicity. Shade coefficient is the third one. Fog water collectors aerodynamic collection efficiency is determined by the knowledge of shade coefficient according to Fernandez et al. (2018) and de Rivera (2011). Shade coefficient has a great impact on fog collection as illustrated by Eq. (1).

$$\eta_{ac} = \frac{s}{1 + \sqrt{\frac{C_o}{C_d}}} \quad (1)$$

where η_{ac} is the aerodynamic efficiency, s is the shade coefficient, C_o and C_d are the mesh pressure drop coefficient and collector drag coefficient respectively.

This article's primary focus is on the shade coefficient computation. A straightforward mathematical technique is proposed to primarily calculate the shade coefficient for rectangular and Raschel mesh. So, it will be simple to apply the same computations to meshes made of triangles or hexagons holes.

Shade coefficient is the ratio between the fibers area and the total external mesh area. It is complementary to free flow area ratio or open area ratio. In some fields, it is also known as porosity. The free flow area ratio is the ratio between the mesh openings area to the total mesh area (de Rivera 2011). Shade coefficient is usually represented as a percentage from 0 to 100%. 0% means no mesh exists. While, 100% means that the mesh is fully impenetrable and is completely opaque to air flow (de Rivera 2011). To calculate the shade coefficient denoted by s for a mesh, Eq. (2) can be utilized.

$$s = 1 - \frac{A_f}{A_t} \quad (2)$$

where A_f and A_t are the mesh opening area and total mesh area respectively.

The fiber thickness, size of the opening hole, external dimensions, and mesh geometry all affect the shade coefficient. Figure 1 explains the concept of shade coefficient and contrasts two meshes with various shade coefficients. External dimensions-wise, they are almost identical. Figure 1a shows thicker fibers, shown as blue lines, and smaller holes, while Fig. 1b shows thinner fibers, seen as thinner lines, and consequently larger holes. For conventional geometric meshes, such as rectangular and Raschel mesh, as well as other shapes, the shade coefficient can be generally determined numerically.

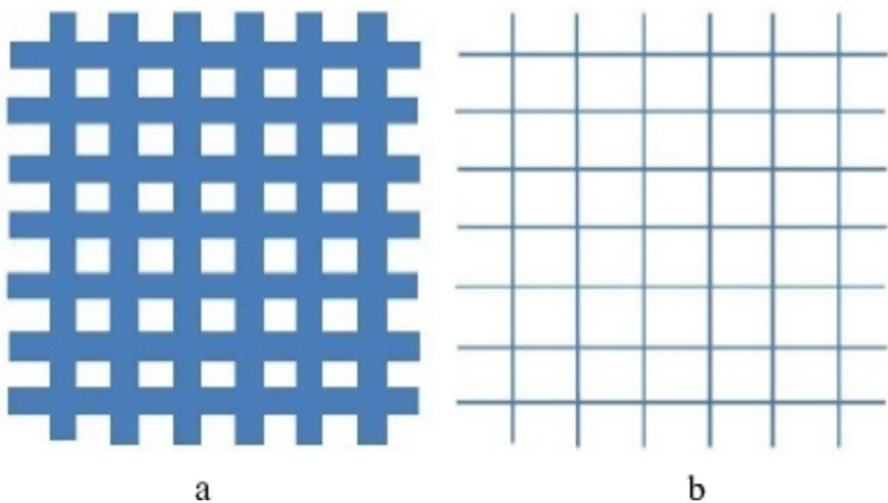


Fig. 1 Typical difference between two rectangular meshes with different shade coefficient. **a** Higher shade coefficient. **b** Lower shade coefficient

Based on the analysis conducted, it was determined, according to our knowledge, that no existing methods have been developed to calculate the shade coefficient of various mesh geometries comparable to the methods described herein. The direct aim of this study is to present a mathematical-deduced straightforward method for calculating the shade coefficient of various mesh shapes. In addition, the validity of the deduced equations was examined when comparing the trendline of the fog collection experiments done by other scientific research papers. The trendline was similar to those papers and all produced the same optimum range.

2 Shade Coefficient of Different Mesh Geometries

In the current work, a simple mathematical way to calculate the shade coefficient for rectangular mesh and Raschel mesh was presented. Subsequently, shade coefficient of square, triangular and hexagonal mesh can be easily deduced.

For all the meshes in this work, it was supposed that the mesh has external dimension width a and height b .

2.1 Rectangular Mesh

Figure 2 depicts the shape of a rectangular mesh. The fog will be caught on the mesh fibers denoted in black lines as shown in Fig. 2, while the uncollected fog together with the air will pass through the permeable holes. A small rectangular hole has an area of xy and the numbers of holes per row and holes per column are n_x and n_y . Fiber has diameter D .

Using Appendix A, the shade coefficient, s can be evaluated as:

$$s = 1 - \frac{x \frac{a-D}{x+D} \cdot y \frac{b-D}{y+D}}{ab} \quad (3)$$

Or

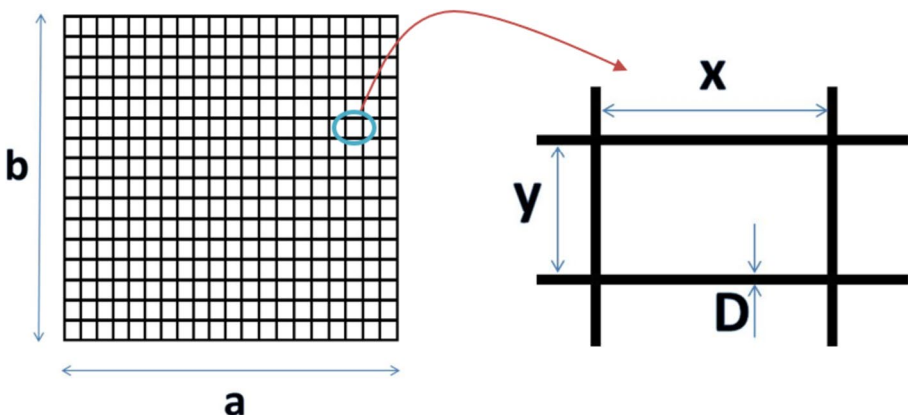


Fig. 2 A typical rectangular mesh with all dimensions

$$s = 1 - \frac{xy(a - D)(b - D)}{ab(x + D)(y + D)} \quad (4)$$

where x and y are rectangular hole dimensions, a and b are external mesh dimensions and D is the mesh fiber diameter.

Equations (3) and (4) are valid for any rectangular mesh. The only dimensions to calculate the shade coefficient are the hole length and width, fiber diameter and mesh width and length.

For a standard fog collector (SFC) 1 m X 1 m mesh (Domen et al. 2014):

$$s = 1 - \frac{xy(1 - D)^2}{(x + D)(y + D)} \quad (5)$$

2.2 Square Mesh

A special case of a rectangular mesh with same dimensions of holes is square mesh, usually called rectangular as well, and will have the dimension x and y equal to each other. So, Eq. (4) can be modified to be:

$$s = 1 - \frac{x^2(a - D)(b - D)}{ab(x + D)^2} \quad (6)$$

2.3 Raschel Mesh

In several nations, like Morocco and Chile, this type of mesh is used to collect fog (Rajaram et al. 2016), (Dodson and Bargach 2015). For example, FogQuest Organization (<https://www.fogquest.org/> n.d.) uses it in a double layer. Raschel mesh is a particular kind of mesh that resembles a trapezoidal network, as shown in Fig. 3. Two assumptions must be taken into account in order to operate on this model. First of all, The mesh is neither assembled or woven. This means that the whole mesh is one component. Subsequently, the mesh can be regarded as regular as all of its holes have the same dimensions and its thickness is constant throughout. Second, the boundary edge might be different from a mesh to another one or a row to row as shown in the boundaries of the mesh in Fig. 3. Consequently, during the modeling steps, the boundaries are

Fig. 3 Raschel mesh (From Rajaram et al. (2016) with permission from Elsevier)



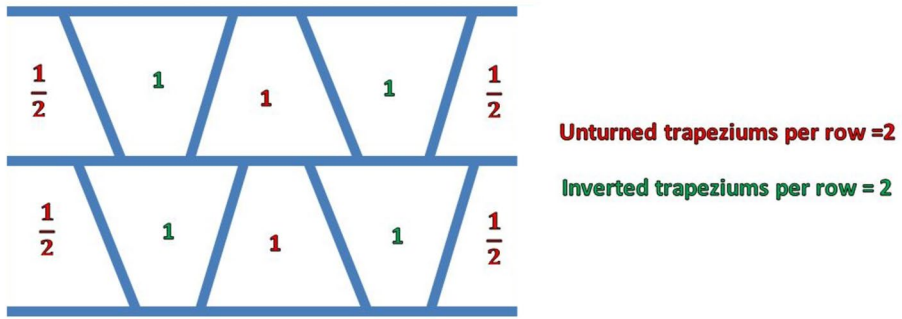


Fig. 4 A Raschel mesh sample with two rows containing two inverted and two unturned trapeziums per row

assumed to be identical to the schematic diagram shown in Fig. 4 with similar edges along each row. If the boundaries is not similar to that in Fig. 4, the assumption is still valid, because the mesh can be 40 m2 area which can make the difference negligible (Fessehaye et al. 2014). The second assumption is valid at the end of the Raschel mesh shade coefficient model equation.

As shown in Fig. 3 the left and right edges are difficult to expect because the mesh might end at the center of the trapezium or at any point in an inverted or unturned trapeziums. However, in order to get a reliable model, we assume that both boundaries are to be at the middle of unturned trapeziums or both at the middle of inverted trapeziums as shown in Fig. 4. This means that there are an even number of trapeziums in each row.

A typical Raschel mesh is made up of several unit cells with the proportions and shape of a trapezium with small and big base dimensions x_s and x_b and height y as seen in Fig. 5. The fiber thickness, t is assumed constant. A small trapezoidal hole has an area of $\frac{1}{2}(x_s + x_b) * y$ and the numbers of holes per row and holes per column are n_x and n_y presented in Eqs. (B1) and (B2) in Appendix B.

Hence, It can be inferred from the sample in Fig. 4 that for an extended mesh, half of the trapeziums will be inverted and the other half would be unturned. The shade coefficient may then be estimated using the previous information.

The shade coefficient of Raschel mesh is:

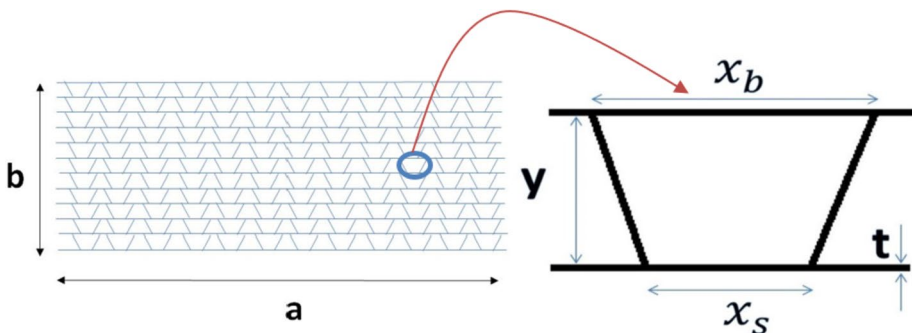


Fig. 5 Raschel mesh comprising small trapezium units

$$s = 1 - \frac{\frac{1}{2}(x_s + x_b)y \cdot \frac{a}{t + \frac{x_s + x_b}{2}} \cdot \frac{b-t}{y+t}}{ab} \quad (7)$$

Or

$$s = 1 - \frac{y(x_s + x_b)(b - t)}{2b(y + t)(t + \frac{x_s + x_b}{2})} \quad (8)$$

where x_s and x_b are trapezoidal hole small and big base, y is the trapezoidal hole height, t is the mesh fiber thickness and a and b are mesh external dimensions.

Appendix B contains the complete formulation of the shade coefficient equation deduction for the Raschel mesh. Equations (7) and (8) are valid for any Raschel mesh. The dimensions of the trapezium holes, the thickness of the fiber, and the height of the mesh a are the only dimensions required to compute the shade coefficient. The boundary assumption we made was correct because, as the mesh goes to infinity, the slight discrepancies at the left and right will vanish. Equation (8) does not include the dimension a .

2.4 Triangular Mesh

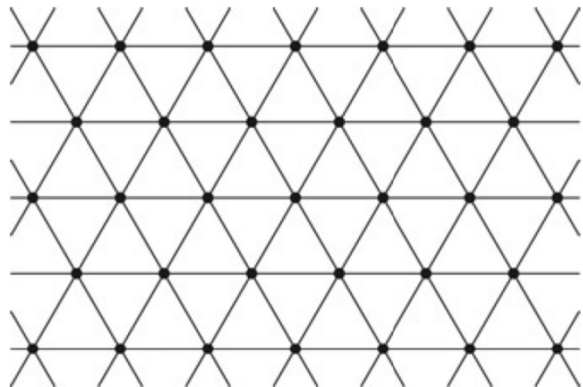
Triangular mesh, shown in Fig. 6, is a mesh that has triangular holes. This triangle may be equilateral, isosceles, or another kind entirely. However, the most reliable shape must be the equilateral shape to have a regular shape and be easily fabricated. To get the shade coefficient of triangular mesh, we assume that it is a special case of Raschel mesh when formed with x_s equal to zero. Triangular mesh can have the same Shade coefficient modeling as the Raschel mesh. The only differences are that x_s turns to be zero as shown in Fig. 7. Therefore, Eq. (8) can be transformed to

$$s = 1 - \frac{x_b \cdot y \cdot (b - t)}{2b(y + t)(t + \frac{x_b}{2})} \quad (9)$$

where x_s and x_b are trapezoidal hole small and big base, y is the trapezoidal hole height, t is the mesh fiber thickness and b is mesh external height.

Equation (9) is valid for any triangular mesh composing of vertical isosceles triangle holes.

Fig. 6 Triangular grid that has the same design as triangular mesh (From Gordon et al. (2008) with permission from Elsevier)



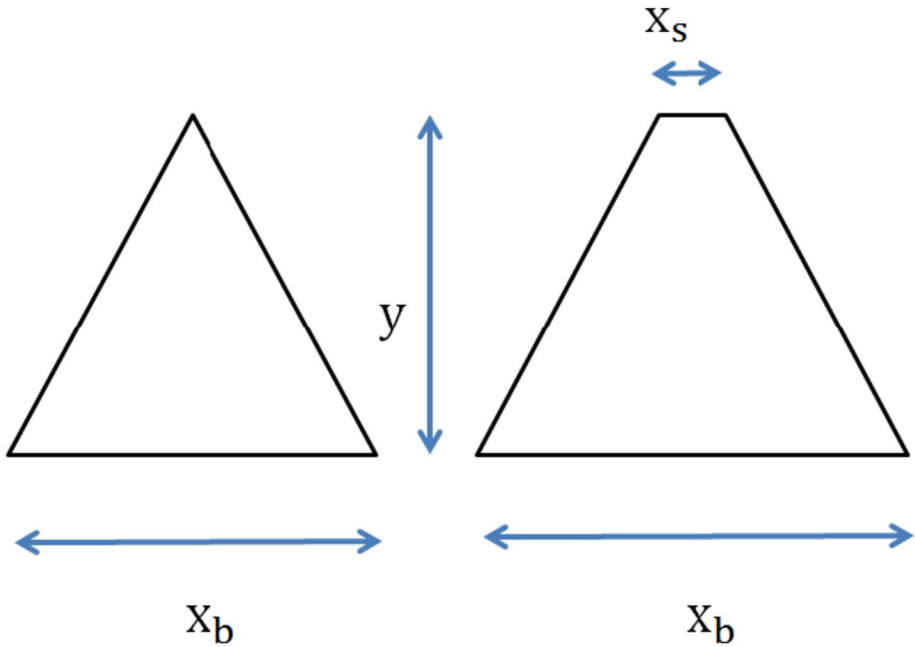


Fig. 7 Difference between triangle and trapezium holes to show the difference between Raschel mesh and triangular mesh

For a 1 m X 1 m mesh:

$$s = 1 - \frac{x_b \cdot y \cdot (1 - t)}{2(y + t)(t + \frac{x_b}{2})} \quad (10)$$

For the triangular mesh, the triangle can also be equilateral triangle with all sides equal in length and all angles are 60° as shown in Fig. 6. So, the height of the triangle y , using trigonometry, will be:

$$y = \frac{x_b}{2} \cdot \tan 60^\circ \quad (11)$$

Or

$$y = \frac{\sqrt{3}}{2} x_b \quad (12)$$

Therefore, after substituting Eq. (12) into Eq. (10), the final equation of triangular mesh is:

$$s = 1 - \frac{x_b^2 \cdot \sqrt{3} \cdot (b - t)}{4b(\frac{\sqrt{3}}{2} x_b + t)(t + \frac{x_b}{2})} \quad (13)$$

2.5 Hexagonal Mesh

The hexagonal shape is composed of hexagonal holes. This shape is used in different engineering areas. For example, Lorente et al. (2002) constructed structures of effective tree-shaped flow by path lengths minimization. In their study, the best elemental shape for the flow between one point and an area was the regular hexagon. Figure 8 illustrates how a hexagonal mesh with open hexagonal regions has the appearance of a beehive.

A small hole in hexagonal mesh will have an area of a regular hexagon with a side length x and a perpendicular distance between two opposite sides is y and the numbers of holes per row and holes per column are n_x and n_y ; respectively. Fiber has thickness t .

Using Appendix C, the shade coefficient for hexagonal mesh can be deduced as follows:

$$s = 1 - \frac{\frac{3\sqrt{3}}{2}x^2 \cdot \frac{a-2t}{1.5x+t} \cdot \frac{b-t}{(\sqrt{3}x+t)}}{ab} \tag{14}$$

or

$$s = 1 - \frac{3\sqrt{3}x^2(a-2t)(b-t)}{2(\sqrt{3}x+t)(1.5x+t)ab} \tag{15}$$

where x is hexagon side length, t is fiber thickness, a and b are external mesh width and height.

3 Mesh Volume and Cost Estimation

Mesh volume can be estimated by multiplying its front projection area by the depth of the mesh. It is assumed that the mesh fibers are rectangular cross section to ease the volume calculation. Hence, the volume of the mesh material will be:

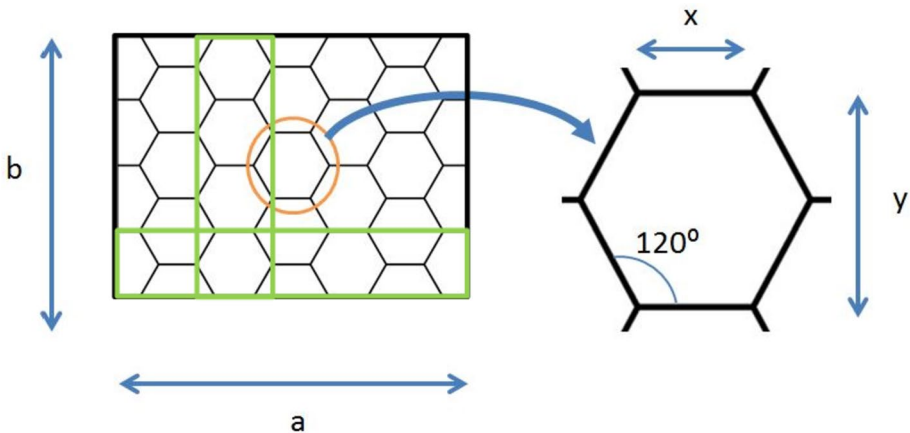


Fig. 8 Hexagonal mesh

$$V = s * ab * d \quad (16)$$

where V is the mesh volume, d is the mesh depth, s is the shade coefficient and a, b are the mesh external dimensions. The mesh material cost can be roughly estimated by knowing the volume of the mesh material used to fabricate the mesh and the cost per unit volume of the mesh as follows:

$$\text{mesh material cost} = \text{cost per } m^3 \text{ material} * \text{mesh volume} \quad (17)$$

The cost of material per m^3 can include manufacturing cost.

4 Applying Rectangular and Raschel Shade Coefficient Model

Rajaram et al. (2016) adopted two rectangular meshes and a Raschel mesh in their fog collection experiment. First rectangular mesh has fiber diameter, t , and pore spacing, x and y , 0.34 and 0.9 mm respectively. Whereas, the second has 0.89 and 2.3 mm respectively. Raschel mesh dimensions are shown in Fig. 9. All the meshes have length a and width b 33 mm and 20 mm respectively.

Applying Eq. (4) for the first and second rectangular meshes and Eq. (8) for the Raschel mesh, we have.

First rectangular mesh:

$$s = 48.7\%$$

Second rectangular mesh:

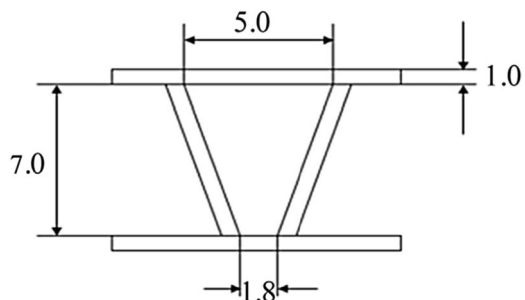
$$s = 51.7\%$$

Raschel mesh:

$$s = 35.8\%$$

Rajaram et al. (2016) carried out fog collection experiments on meshes of different shade coefficient and various shapes yielding different fog collection rate. This means that the shade coefficient and mesh geometry are of great influence on fog collection rate.

Fig. 9 Raschel mesh dimensions in millimeters (From Rajaram et al. (2016) with permission from Elsevier)



5 Fog Collection Experiment

Fog collection experiment was carried on 10 rectangular stainless-steel round PARSROS sieves (meshes) of diameter 30 cm with various shade coefficients as shown in Fig. 10 to verify that the shade coefficient is a key parameter for fog collection. A fog machine capable of pressurizing water to 70 bar connected with flexible pipes and two nozzles of 100 μm diameter that spray the water as small diameter water droplets. The nozzles are fixed at the start of a 50 cm length 15 cm internal diameter L-pipe and the mesh is fixed 27 cm from the exit of the L-pipe.

Water droplets can be collected then by the mesh supported at the end of the L-pipe. Table 1 displays the meshes' measurements. The shade coefficient of all the rectangular meshes was calculated using shade coefficient formula for rectangular mesh Eq. (4). The sieve has a round frame and the executed Eq. (4) is for a rectangular frame mesh. Hence, the sieve was modeled as a square frame mesh with an equivalent area.

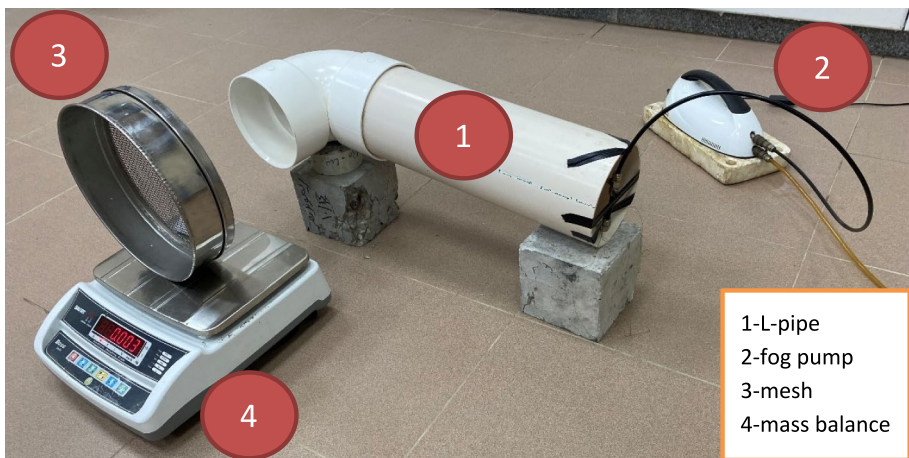
A system was set up as shown in Fig. 11. The fog enters the pipe until it exits to strike with the fixed mesh. The pipe was designed to be bent in order to ensure that all large droplets are settled and lowered down in the pipe and that only the smallest water fog droplets would continue until the exit of the pipe as a mean of natural fog simulation. For each mesh while it was exposed to the fog generation unit for 9 min, the mass of water collected for each mesh was measured using a balance with a sensitivity of ± 1 gm.

Fig. 10 Sample sieve of the target meshes



Table 1 Dimensions and shade coefficient of the investigated meshes

Mesh number	Opening x, y mm	Fiber thickness D mm	Mesh frame diameter mm	Length a mm	Width b mm	shade coefficient s %
1	31.5	4.23	300	265.9	265.9	24.7%
2	22.4	3.5	300	265.9	265.9	27.2%
3	16	3	300	265.9	265.9	30.7%
4	11.2	2.54	300	265.9	265.9	34.8%
5	8	2.07	300	265.9	265.9	37.9%
6	5.6	1.68	300	265.9	265.9	41.6%
7	4	1.37	300	265.9	265.9	45.1%
8	2	0.9	300	265.9	265.9	52.8%
9	1	0.58	300	265.9	265.9	60.1%
10	0.5	0.34	300	265.9	265.9	64.7%

**Fig. 11** The system of fog collection**Table 2** The fog collection outcome of the carried-out experiment

	1	2	3	4	5	6	7	8	9	10
Shade coefficient s %	24.7%	27.2%	30.7%	34.8%	37.9%	41.6%	45.1%	52.8%	60.1%	64.7%
Water collected in grams	19	23	28	30	32	34	34	42	38	33

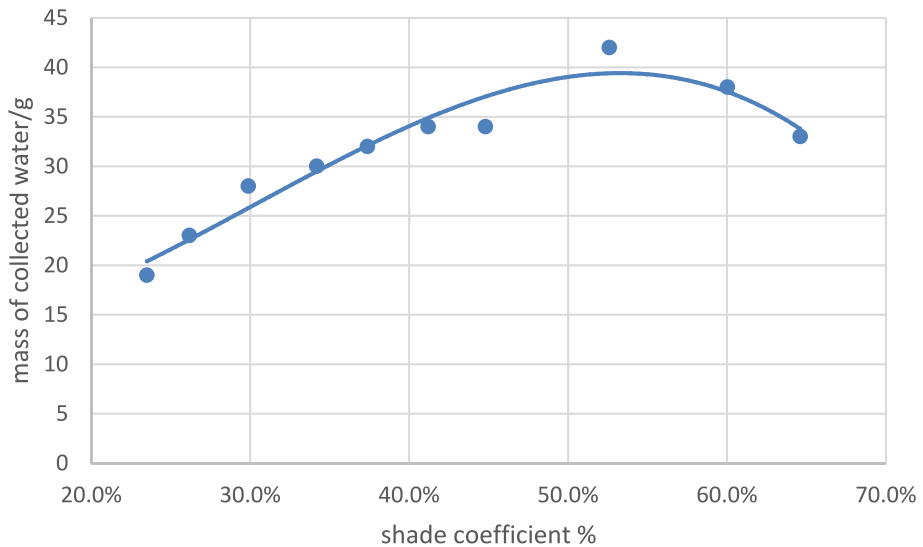


Fig. 12 Effect of shade coefficient on mass of collected water

6 Results and Discussion

The experiments' results, which are the quantity of collected water measured in grammes, are shown in Table 2. Figure 12 displays how much water was gathered by each mesh during the 9-min experiments. Due to variations in mesh shade coefficient, the results demonstrate differences in the amount of water collected by each mesh. The optimum shade coefficient was noticed in the range of 50–60% similar to that was deduced by Mahat et al. (2019). The cumulative mass of water collected was also recorded at the end of each minute for each mesh in grams and the data are plotted on the graph shown in Fig. 13.

The variance in shade coefficients is what causes the variation in water collection rates. For the meshes of shade coefficient less than 50%, the higher the shade coefficient, the higher the fog collision with the mesh fibers, the more the water captured by the fibers, the more the fog water collected. When fog is facing a mesh with a higher shade coefficient than 60%, the projected area of the mesh fibers is big and acts as an obstruction, preventing fog from passing through, and the holes are small. As a result, the fog is forced to travel around the mesh rather than through the openings in the mesh. Hence less water collected by the mesh. The range of shade coefficient from 50 to 60% are the most suitable to the optimum fog water collection because there are enough large and many fibers to effectively catch fog. At the same time, not too much to prevent the passage of fog.

The trendline of the relation between shade coefficient and mass of collected water in the performed system is similar to the trendline of the fog collection efficiency curve executed by de Rivera (2011) and Mahat et al. (2019) as shown in Fig. 14. Rivera et al. executed the green curve for the efficiency of fog collection for a flat rectangular mesh with aspect ratio 5 versus shade coefficient. Mahat et al. deduced the blue curve, the efficiency of fog collection for wire mesh versus shade coefficient. In this study, the red curve was deduced, the quantity of water collected by the mesh for 9 min versus shade coefficient of the mesh.

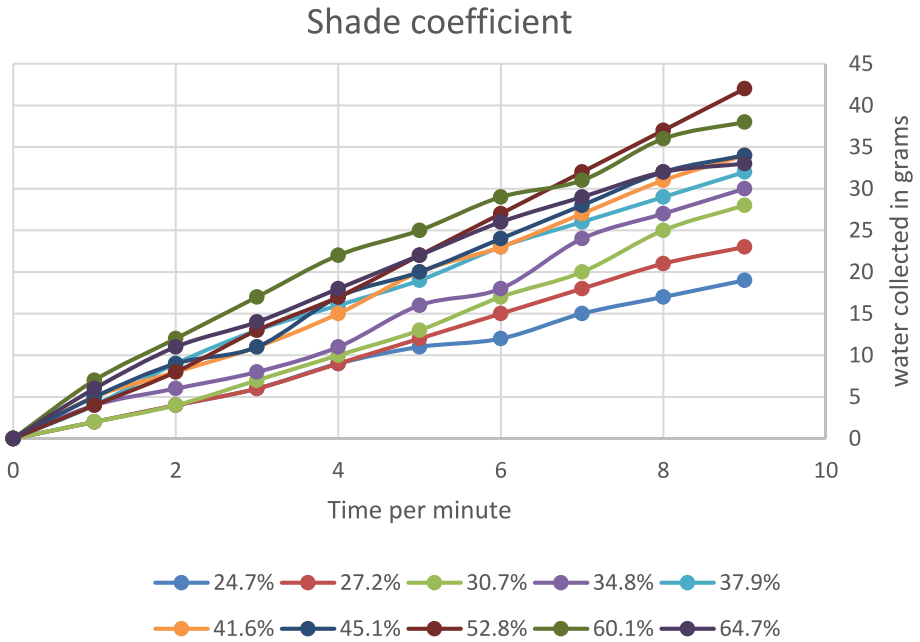


Fig. 13 Accumulated mass of water for different mesh shapes

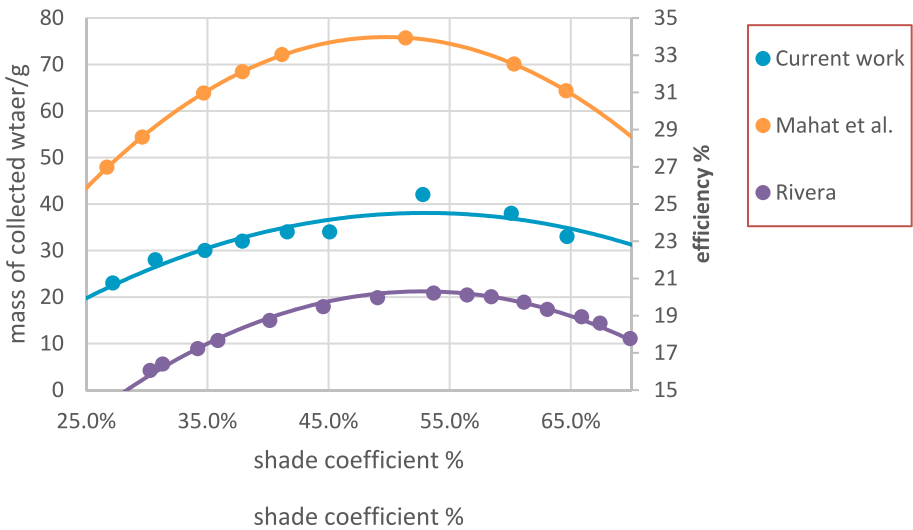


Fig. 14 The trendlines of fog collection with regard to the shade coefficient for Rivera, Mahat and present study

The high degree of symmetry between the three curves indicates that the shade coefficient employed in the rectangular mesh calculation model is appropriate for effective fog collection. The mass M of water collected for the investigated system can be predicted for a rectangular mesh with shade coefficient s using the Eq. (18).

$$M = -573.31s^3 + 524.56s^2 - 69.283s + 14.198 \quad (18)$$

7 Conclusion

In summary, this study developed a straightforward mathematical model that can be used to calculate the fog collection mesh shade coefficient, a crucial process control parameter, for various mesh shapes. This model can be applied in other engineering applications and scientific fields, providing a quick and efficient way to predict the shade coefficient without the need for time-consuming measurements. Researchers can use this method to calculate the mesh shade coefficient and conduct experiments on different meshes with varying shade coefficients to determine the most efficient shade coefficient for fog harvesting. Furthermore, the proposed mathematical model can help determine which mesh is more preferred and less expensive for a specific shade coefficient, as well as estimate the mesh's volume and cost using two simple formulae. Finally, the experimental results demonstrated that stainless steel rectangular meshes with a shade coefficient between 50 and 60 percent are the most efficient for fog collection.

Appendix A

A small hole will have an area of xy and the numbers of holes per row and holes per column are n_x and n_y . Fiber has diameter D .

The length a and b will be:

$$a = xn_x + D(n_x + 1) \quad (A1)$$

$$b = yn_y + D(n_y + 1) \quad (A2)$$

Then, we can get n_x and n_y as the subject of formulae.

$$n_x = \frac{a - D}{x + D} \quad (A3)$$

$$n_y = \frac{b - D}{y + D} \quad (A4)$$

The number of all the holes which is the free area A_f of the mesh can be calculated by the following equation.

$$A_f = xy \cdot n_x \cdot n_y \quad (A5)$$

Then, substituting Eqs. (A3) and (A4) into Eq. (A5) to derive the final free area:

$$A_f = xy \cdot \frac{a-D}{x+D} \cdot \frac{b-D}{y+D} \quad (\text{A6})$$

The mesh total area A_t is equivalent to

$$A_t = ab \quad (\text{A7})$$

rearranging Eqs. (A6) and (A7) into Eq. (2) for shade coefficient:

$$s = 1 - \frac{x \frac{a-D}{x+D} \cdot y \frac{b-D}{y+D}}{ab} \quad (\text{A8})$$

Or

$$s = 1 - \frac{xy(a-D)(b-D)}{ab(x+D)(y+D)} \quad (\text{A9})$$

Appendix B

A small hole in Raschel mesh will have an area of a trapezium with small and big base dimensions x_s and x_b and height y . and the numbers of holes per row and holes per column are n_x and n_y . Fiber has thickness t .

$$a = x_s \frac{n_x}{2} + x_b \frac{n_x}{2} + t \cdot n_x \quad (\text{B1})$$

$$b = yn_y + t(n_y + 1) \quad (\text{B2})$$

We can then get n_x and n_y as the subject of formulae.

$$n_x = \frac{a}{t + \frac{x_s+x_b}{2}} \quad (\text{B3})$$

$$n_y = \frac{b-t}{y+t} \quad (\text{B4})$$

The total area of all the holes which form the mesh free area A_f can be calculated by the following equation:

$$A_f = \frac{1}{2} (x_s + x_b) y \cdot n_x \cdot n_y \quad (\text{B5})$$

Then, Eqs. (B3) and (B4) can be substituted in Eq. (B5) to derive the final free area:

$$A_f = \frac{1}{2} (x_s + x_b) y \cdot \frac{a}{t + \frac{x_s+x_b}{2}} \cdot \frac{b-t}{y+t} \quad (\text{B6})$$

The mesh total area A_t is equivalent to

$$A_t = ab \quad (\text{B7})$$

Substituting Eqs. (B6) and (B7) into Eq. (2) for shade coefficient

$$s = 1 - \frac{\frac{1}{2}(x_s + x_b)y \cdot \frac{a}{t + \frac{x_s + x_b}{2}} \cdot \frac{b-t}{y+t}}{ab} \quad (\text{B8})$$

Or

$$s = 1 - \frac{y(x_s + x_b)(b-t)}{2b(y+t)(t + \frac{x_s + x_b}{2})} \quad (\text{B9})$$

Appendix C

A small hole in hexagonal mesh will have an area of a regular hexagon with a side length x and a perpendicular distance between two opposite sides is y . and the numbers of holes per row and holes per column are n_x and n_y . Fiber has thickness t .

By counting the number of hexagons per row and column, can be counted easily by following the vertical and horizontal green bounded rectangles in Fig. 8, the length a and b will be:

$$a = 1.5n_x x + (n_x + 2)t \quad (\text{C1})$$

$$b = yn_y + t(n_y + 1) \quad (\text{C2})$$

Then, n_x and n_y can be obtained as the subject of formulae.

$$n_x = \frac{a - 2t}{1.5x + t} \quad (\text{C3})$$

$$n_y = \frac{b - t}{y + t} \quad (\text{C4})$$

The area of all the holes which is the free area A_f of the mesh can be calculated by the following equation.

$$A_{\text{hex}} = \frac{3\sqrt{3}}{2}x^2 \quad (\text{C5})$$

$$A_f = A_{\text{hex}} \cdot n_x \cdot n_y \quad (\text{C6})$$

where A_{hex} is the area a regular hexagon with the above dimensions.

Then, Eqs. (C3) and (C4) and (C5) can be substituted into Eq. (C6) to derive the final free area:

$$A_f = \frac{3\sqrt{3}}{2}x^2 \cdot \frac{a - 2t}{1.5x + t} \cdot \frac{b - t}{y + t} \quad (\text{C7})$$

The mesh total area A_t is equivalent to

$$A_t = ab \quad (\text{C8})$$

Substituting Eqs. (C7) and (C8) into Eq. (2) for shade coefficient:

$$s = 1 - \frac{\frac{3\sqrt{3}}{2}x^2 \cdot \frac{a-2t}{1.5x+t} \cdot \frac{b-t}{y+t}}{ab} \quad (\text{C9})$$

From trigonometry,

$$y = x \tan 60 = \sqrt{3}x \quad (\text{C10})$$

Substituting Eq. (C10) into Eq. (C9) result into:

$$s = 1 - \frac{\frac{3\sqrt{3}}{2}x^2 \cdot \frac{a-2t}{1.5x+t} \cdot \frac{b-t}{(\sqrt{3}x+t)}}{ab} \quad (\text{C11})$$

or

$$s = 1 - \frac{3\sqrt{3}x^2(a-2t)(b-t)}{2(\sqrt{3}x+t)(1.5x+t)ab} \quad (\text{C12})$$

Authors Contributions All authors contributed to the study conceptualization and design. Material was prepared by Abdullah A. Elshennawy. Data collection and analysis were performed by Abdullah A. Elshennawy. The first draft of the manuscript was written by Abdullah A. Elshennawy. The first draft of the manuscript was reviewed by Magdy Y. Abdelaal, Ahmed A. Hamed, and Mohamed M. Awad. All authors read and approved the final manuscript.

Funding Open access funding provided by The Science, Technology & Innovation Funding Authority (STDF) in cooperation with The Egyptian Knowledge Bank (EKB). No funding was received to assist with the preparation of this manuscript.

Availability of Data and Materials Data and materials are available upon request.

Declarations

Ethical Approval All authors certify that they have no affiliations with or involvement in any organization or entity with any financial interest or non-financial interest in the subject matter or materials discussed.

Consent to Participate Informed consent was obtained from all individual participants included in the study.

Consent to Publish The participants have consented to the submission of the paper to the journal.

Competing Interests The authors declare that they have no known conflict of interest.

Open Access This article is licensed under a Creative Commons Attribution 4.0 International License, which permits use, sharing, adaptation, distribution and reproduction in any medium or format, as long as you give appropriate credit to the original author(s) and the source, provide a link to the Creative Commons licence, and indicate if changes were made. The images or other third party material in this article are included in the article's Creative Commons licence, unless indicated otherwise in a credit line to the material. If material is not included in the article's Creative Commons licence and your intended use is not


permitted by statutory regulation or exceeds the permitted use, you will need to obtain permission directly from the copyright holder. To view a copy of this licence, visit <http://creativecommons.org/licenses/by/4.0/>.

References

- Abu El-Maaty AE, Awad MM, Sultan GI, Hamed AM (2019) Solar powered fog desalination system. *Desalination* 472. <https://doi.org/10.1016/j.desal.2019.114130>
- Abu El-Maaty AE, Awad MM, Sultan GI, Hamed AM (2021) Performance study of fog desalination system coupled with evacuated tube solar collector. *Desalination* 504. <https://doi.org/10.1016/j.desal.2021.114960>
- Al-hassan GA (2009) Fog water collection evaluation in Asir region - Saudi Arabia. *Water Resour Manag* 23(13). <https://doi.org/10.1007/s11269-009-9410-9>
- Alotaibi M, Alhajeri NS, Al-Fadhli FM, Al Jabri S, Gabr M (2023) Impact of climate change on crop irrigation requirements in arid regions. *Water Resour Manag*. <https://doi.org/10.1007/s11269-023-03465-5>
- Awad K, Awad M, Kandel A (2020) Extraction of water from atmospheric air using double slope condensation surface. *Bull Fac Eng, Mansoura Univ* 42(1):1. <https://doi.org/10.21608/bfemu.2020.97651>
- Chitsaz N, Azarnivand A (2017) Water scarcity management in arid regions based on an extended multiple criteria technique. *Water Resour Manag* 31(1). <https://doi.org/10.1007/s11269-016-1521-5>
- de Rivera J, D. (2011) Aerodynamic collection efficiency of fog water collectors. *Atmos Res* 102(3):335–342. <https://doi.org/10.1016/j.atmosres.2011.08.005>
- Dodson LL, Bargach J (2015) Harvesting fresh water from fog in rural Morocco: Research and impact Dar Si Hmad's Fogwater Project in Ait Baamrane. *Procedia Eng* 107:186–193. <https://doi.org/10.1016/j.proeng.2015.06.073>
- Domen JK, Stringfellow WT, Camarillo MK, Gulati S, Kay M, Shelly C (2014) Fog water as an alternative and sustainable water resource. *Clean Technol Environ Policy* 16:235–249. <https://doi.org/10.1007/s10098-013-0645-z>
- Elshennawy AA, Awad MM, Abdelal MY, Hamed AM (2022) Fog collection - materials, techniques and affecting parameters - A review. *Seafic J* 2(2):102–127
- Fathy MH, Awad MM, Zeidan ESB, Hamed AM (2020) Solar powered foldable apparatus for extracting water from atmospheric air. *Renew Energy* 162. <https://doi.org/10.1016/j.renene.2020.07.020>
- Fernandez DM, Torregrosa A, Weiss-Penzias PS, Zhang BJ, Sorensen D, Cohen RE, McKinley GH, Kleingartner J, Oliphant A, Bowman M (2018) Fog water collection effectiveness: Mesh intercomparisons 18(1):270–283
- Fessehaye M, Abdul-Wahab SA, Savage MJ, Kohler T, Gherezghiher T, Hurni H (2014) Fog-water collection for community use. *Renew Sustain Energy Rev* 29:52–62. <https://doi.org/10.1016/j.rser.2013.08.063>
- FogQuest: Sustainable Water Solutions (n.d.). <http://www.fogquest.org/>. Accessed 25 Oct 2023
- Gordon VS, Orlovich YL, Werner F (2008) Hamiltonian properties of triangular grid graphs. *Discret Math*. <https://doi.org/10.1016/j.disc.2007.11.040>
- Guo Z, Liu W, Su BL (2011) Superhydrophobic surfaces: From natural to biomimetic to functional. *J Colloid Interface Sci* 353(2):335–355. <https://doi.org/10.1016/j.jcis.2010.08.047>
- Lorente S, Wechsattel W, Bejan A (2002) Tree-shaped flow structures designed by minimizing path lengths. *Int J Heat Mass Transf* 45(16). [https://doi.org/10.1016/S0017-9310\(02\)00051-0](https://doi.org/10.1016/S0017-9310(02)00051-0)
- Mahat S, Kumar A, Darlami K (2019) Study of fog water collector mesh with different shade coefficients study of fog water collector mesh with different shade coefficients. *Proceedings of IOE Graduate Conference, 2019-Summer* 6:389–394. ISSN: 2350-8914 (Online), 2350-8906 (Print). https://www.researchgate.net/publication/344680542_Study_of_Fog_Water_Collector_Mesh_with_Different_Shade_Coefficients
- Mekonnen MM, Hoekstra AY (2016) Four billion people facing severe water scarcity. *Am Assoc Adv Sci*. <https://doi.org/10.1126/sciadv.1500323>
- Rajaram M, Heng X, Oza M, Luo C (2016) Enhancement of fog-collection efficiency of a Raschel mesh using surface coatings and local geometric changes. *Colloids Surf, A* 508:218–229. <https://doi.org/10.1016/j.colsurfa.2016.08.034>
- Rijsberman FR (2006) Water scarcity: Fact or fiction? *Agric Water Manag* 80(1–3 SPEC. ISS.). <https://doi.org/10.1016/j.agwat.2005.07.001>
- Talaat MA, Awad MM, Zeidan EB, Hamed AM (2018) Solar-powered portable apparatus for extracting water from air using desiccant solution. *Renew Energy* 119. <https://doi.org/10.1016/j.renene.2017.12.050>

Publisher's Note Springer Nature remains neutral with regard to jurisdictional claims in published maps and institutional affiliations.

Authors and Affiliations

Abdullah A. Elshennawy^{1,2} · **Magdy Y. Abdelaal**³ · **Ahmed M. Hamed**¹ · **Mohamed M. Awad**¹ 

✉ Mohamed M. Awad
m_m_awad@mans.edu.eg

Abdullah A. Elshennawy
ashennawy@horus.edu.eg

Magdy Y. Abdelaal
myabdelaal@gmail.com

Ahmed M. Hamed
amhamed@mans.edu.eg

¹ Mechanical Power Engineering Department, Faculty of Engineering, Mansoura University, Mansoura 35516, Egypt

² Mechatronics Engineering Department, Faculty of Engineering, Horus University, New Damietta, Damietta 34518, Egypt

³ Chemistry Department, Faculty of Science, Mansoura University, Mansoura 35516, Egypt